3D Image quality improvement for optical projection tomography via point spread function modelling

Tang, X.; Lamers, G.E.M.; Verbeek, F.J.

3D Image Quality Improvement for Optical Projection Tomography via Point Spread Function Modelling

Xiaoqin Tang[1], Gerda E.M. Lamers[2] and Fons J. Verbeek[1]
[1]*Leiden Institute of Advanced Computer Science, Leiden University, 2333 CA Leiden, Netherlands.,*
[2] *Institute of Biology Leiden, Leiden University, 2333 BE Leiden, Netherlands.*

Abstract: We present a method to model the 3D point spread function in optical projection tomography imaging system, which subsequently contributes to the improvement of 3D image quality. Experiments are implemented on several 3D images of zebrafish embryos.
Key Words: Deconvolution; OPT 3D imaging; PSF modelling

1. Introduction to 3D image quality improvement

Optical projection tomography (OPT) [1] is a typical optical 3D imaging technique for objects at tissue-, organ- and organism-level in the magnitude range of millimeters. For OPT imaging and reconstruction, the depth of field (DOF) is expected to be large enough to contain as much of the sample as possible. In this manner the parts of the sample located in the DOF will result in an image more or less in focus. According to the previous studies [2, 3], however, large DOF subsequently produces image blur and results in low in-focus image quality. The image quality in this paper is also referred as image resolution in some literatures. A lens with small numerical aperture (NA) will produce large DOF, allowing imaging of larger samples but it will result in a relatively low-quality image.

In this paper, we are making a contribution by modeling the experimental PSF of a single bead along optical axis, thereby considering the interaction of contiguous slices from the reconstructed volume. At the same time, the magnification is taken into account in an experimental manner. The modelled PSF is consequently applied to 3D image deconvolution. The focus of this paper is presenting the concept of PSF modeling and coronal deconvolution on 3D OPT data accompanied by some initial experimental results based on 11 3D images of zebrafish. Further evaluations on a larger number of data are the topics of our current research.

2. Methodology

The image acquisition is accomplished by a rotation of the specimen driven by a stepper unit; the stepper moves 0.9°per step and it results in 400 images per revolution with size 1360×1036 pixel. The OPT imaging system has two modules: bright-field and fluorescence imaging.

2.1 PSF modelling with different magnifications

The 3D PSF of a OPT imaging system based on a single fluorescent bead is acquired and modelled as illustrated in Fig.1.

According to convention [4] the imaging PSF is assumed as a focused 3D Gaussian-like beam. We generalize the model by employing parameters ρ_1, ρ_2 and ρ_3 as:

$$p(s,t,d) = \rho_1 \cdot \frac{1}{2\pi\sigma(d)^2} \cdot \exp\left(-\frac{s^2+t^2}{2\sigma(d)^2}\right)^{\rho_2} + \rho_3 \quad (1)$$

Instead of equalizing the beam waist and standard deviation $\sigma(d)$ as described in [4, 5], we investigate the relationship between them by multiplying a parameter a with beam waist, considering different magnifications.

$$\sigma(d) = a \cdot \sqrt{\sigma_0^2 + \left(\frac{\lambda d}{\pi\sigma_0}\right)^2} \quad (2)$$

To relate the beam waist in focus σ_0 as well as the parameter a to the magnification, 6 magnifications ($12.5\times$, $15.0\times$, $17.5\times$, $20.0\times$, $22.5\times$, $25.0\times$) are configured to acquire the images of the same bead. The magnification of $12.5\times$ approximately corresponds to the minimum magnification that makes the bead visible in our experiment, while $25.0\times$ approximate to the maximum magnification that confirms that the bead in a full revolution is in the field of view (FOV). By using the modelling method with an overall fitting error of 5.0%, parameters ρ_1 to ρ_3 are proved to be constant regardless of magnifications: $\rho_1 \approx 0.0041$, $\rho_2 \approx 1.0549$ and $\rho_3 \approx 2.9 \times 10^{-5}$. The beam waist in

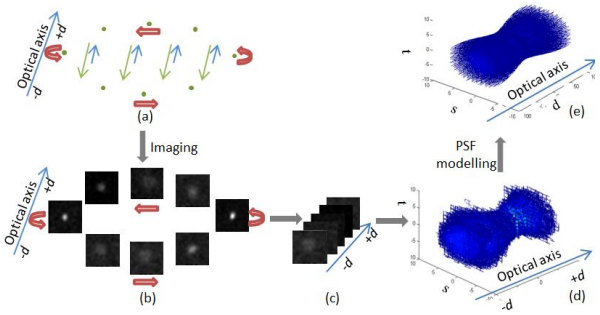

Fig. 1. 3D PSF acquisition and modelling. (a) The light path of the OPT imaging system that passes through GFP beads. The excitation beams and emission beams are separately shown in blue and green arrows. The red arrows indicate the revolution of the single fluorescent bead. (b) Images of the single bead acquired at different angles. (c) Images of the single bead stacked according to the defocus. (d) The experimental PSF with defocus from $-r_b$ to $+r_b$. (e) The modelled PSF with defocus from $-\infty$ to $+\infty$.

focus σ_0 and the parameter a relevant to the 6 magnifications are estimated and fitted as an exponential and a quadratic function, minimizing the fitting error on the observation data. The PSF of any 3D image with the focal plane set at the rotation center can be modelled as depicted in this section. For system with shifted focal plane, the same shift should be considered in PSF along the optical axis.

2.2 Deconvolution of 3D images

The 3D image is deconvolved slice by slice along its depth that is parallel to the optical axis as follows:

$$D_{(x,y,d)} = R_{(x,y,d)} *\!/\!* p_{(s,t,d)} \quad (3)$$

R is the 3D image with the depth d parallel to the optical axis of the PSF. $*\!/\!*$ is the operation of deconvolution. Concerning the shifted focal plane and reconstruction symmetry, deconvolution of R', the opposite view of R projected along d, is executed by applying $D'_{(x,y,d)} = R'_{(x,y,d)} *\!/\!* p_{(s,t,d)}$. The 3D image with the deconvolution is achieved by combining D and 180° back rotation of D'.

3. Experiments

We first show a qualitative comparison in Fig. 2 with the proposed deconvolution on a sample from a 3dpf batch of zebrafish larvae in fluorescence module.

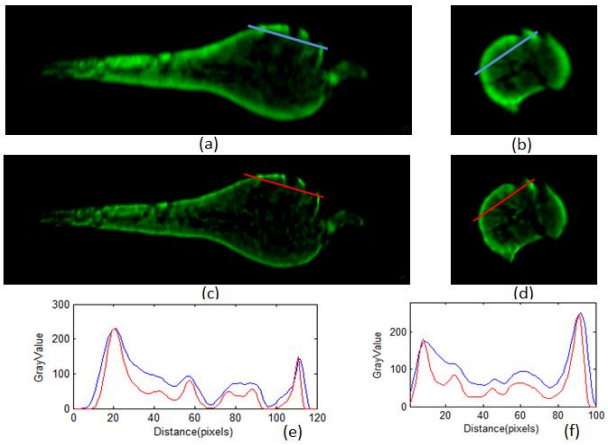

Fig. 2. Coronal and horizontal slices of 3D zebrafish before ((a) and (b)) and after ((c) and (d)) deconvolution. The deconvolution highlights the strong signals and makes the texture more visible. The figure below (a) and (c) compares the intensity profile of the same line before (blue) and after (red) deconvolution, so does the figure below (b) and (d).

To quantify the improvement of the deconvolution on the reconstructed 3D image across planes, we present the 3D image quality improvement criterion as I_{3d} in Eq. (4). Improvement in three orthogonal individuals are combined and encoded as a whole and each of them are represented as Eq. (5) to Eq. (7). M_{ix}^{d} and M_{ix}^{r} are the image quality measures of the ith deconvolved and non-deconvolved slice in x plane respectively. By employing I_{3d}, deconvolution performance of two different methods on the same data turns to be comparable.

$$I_{3d} = \sqrt{\left(\frac{1}{Nx}\sum_{ix=1}^{Nx} I_{ix}\right)^2 + \left(\frac{1}{Ny}\sum_{iy=1}^{Ny} I_{iy}\right)^2 + \left(\frac{1}{Nz}\sum_{iz=1}^{Nz} I_{iz}\right)^2} \quad (4)$$

$$I_{ix} = \frac{M_{ix}^{d} - M_{ix}^{r}}{M_{ix}^{r}} \quad (5)$$

$$I_{iy} = \frac{M_{iy}^{d} - M_{iy}^{r}}{M_{iy}^{r}} \quad (6)$$

$$I_{iz} = \frac{M_{iz}^{d} - M_{iz}^{r}}{M_{iz}^{r}} \quad (7)$$

In this section we implement our deconvolution method on 10 more 3D image of zebrafish embryo. It is important to know that the measurements in the paper cannot assess the image quality across different samples, but it provides a convincing evaluation of image quality on the same sample. Benefiting from this, we compares the presented deconvolution method with the most commonly used Gaussian-based blind deconvolution. The Gaussian kernel size is set as 7 for all slices. Lucy-Richardson with iteration of 20 is applied to deconvolution implement for both methods. The robust measure just noticeable blur (JNB) [6] is employed to evaluate the image quality of a single slice regarding image blur. The results of the comparison are presented in Table1. For all the 10 zebrafish, our deconvolution approach significantly outperforms the Gaussian-based deconvolution, explaining the value of our work.

Table 1. 3D image quality improvement I_{3d} of 10 zebrafish embryos based on JNB Measure

	No.1	No.2	No.3	No.4	No.5	No.6	No.7	No.8	No.9	No.10
Gaussian	0.22	0.20	0.23	0.17	0.22	0.19	0.19	0.17	0.20	0.23
Ours	**0.85**	**0.95**	**0.61**	**1.59**	**0.86**	**0.73**	**0.89**	**0.88**	**0.79**	**0.85**

4. References

[1] Sharpe, J. *et al.* Optical projection tomography as a tool for 3D microscopy and gene expression studies. *Science (80-.).* 296, 541–545 (2002).

[2] Walls, J. R., Sled, J. G., Sharpe, J. & Henkelman, R. M. Resolution improvement in emission optical projection tomography. *Phys. Med. Biol.* 52, 2775 (2007).

[3] McNally, J. G., Karpova, T., Cooper, J. & Conchello, J. A. Three-dimensional imaging by deconvolution microscopy. *Methods* 19, 373–385 (1999).

[4] Kogelnik, H. & Li, T. Laser Beams and Resonators. *Proc. IEEE* 54, 1312–1329 (1966).

[5] van der Horst, J. & Kalkman, J. Image resolution and deconvolution in optical tomography. *Opt. Express* 24, 24460–24472 (2016).

[6] Ferzli, R. & Karam, L. J. A no-reference objective image sharpness metric based on the notion of Just Noticeable Blur (JNB). *IEEE Trans. Image Process.* 18, 717–728 (2009).